



A pulse sequence for singlet to heteronuclear magnetization transfer: S2hM



Gabriele Stevanato^{a,b}, James Eills^a, Christian Bengs^a, Giuseppe Pileio^{a,*}

^a Chemistry, University of Southampton, Southampton, United Kingdom

^b Institut des Sciences et Ingénierie Chimiques, Ecole Polytechnique Fédérale de Lausanne (EPFL), CH-1015 Lausanne, Switzerland

ARTICLE INFO

Article history:

Received 27 January 2017

Revised 28 February 2017

Accepted 3 March 2017

Available online 6 March 2017

Keywords:

Singlet state

Hyperpolarization

Polarization transfer

M2S

S2hM

ABSTRACT

We have recently demonstrated, in the context of para-hydrogen induced polarization (PHIP), the conversion of hyperpolarized proton singlet order into heteronuclear magnetisation can be efficiently achieved via a new sequence named S2hM (Singlet to heteronuclear Magnetisation). In this paper we give a detailed theoretical description, supported by an experimental illustration, of S2hM. Theory and experiments on thermally polarized samples demonstrate the proposed method is robust to frequency offset mismatches and radiofrequency field inhomogeneities. The simple implementation, optimisation and the high conversion efficiency, under various regimes of magnetic equivalence, makes S2hM an excellent candidate for a widespread use, particularly within the PHIP arena.

© 2017 The Authors. Published by Elsevier Inc. This is an open access article under the CC BY license (<http://creativecommons.org/licenses/by/4.0/>).

1. Introduction

Nuclear magnetic resonance (NMR) offers a privileged observatory for the local chemical environment of nuclear spin species and has been widely used for the characterization of molecules and their dynamics in the liquid state. However, experimental polarisation values in the order of $\sim 10^{-5}$ and relatively short T_1 decay times (a few tens of seconds at best, for ^1H in room temperature solutions) are the two Achilles' heels that many strategies try to overcome.

Hyperpolarisation techniques have been developed to enhance signal strength [1–9] and long-lived spin states have been shown to prolong the lifetime of hyperpolarized nuclear spins [10–13,7,15,8,16–21,14,22–24].

Within the field of hyperpolarisation, the introduction of para-hydrogen induced polarization [2] (PHIP) allowed for dramatically enhanced proton signals, and introduced the challenge of transferring polarization from hyperpolarized proton singlet order, which is the population imbalance between the singlet and the average triplet manifolds [35], to heteronuclei with a longer T_1 . This problem quickly attracted attention and emerged as a prolific investigation area [25–27], and several methods have been developed to perform the task [28–30,26].

Singlet order is also the main objective in the research field of LLS (Long-Lived States). Therefore, it is probably of no surprise that recently the Levitt group showed how the spin-lock induced crossing (SLIC) method [32], originally presented in the LLS context, can be used to achieve polarization transfer by means of weak RF excitation with an amplitude corresponding to the proton-proton J coupling [33].

On the same topic, one of us proposed the ADAPT pulse sequence [34], a hard-pulse version of SLIC based on the repeated alternation of RF pulses and delays. ADAPT is convenient because it accomplishes the singlet to heteronuclear order transformation with good efficiency, under a broad range of magnetic equivalence conditions, and faster than any previous hard-pulse based method. A major disadvantage, common to other techniques widely used in PHIP research [29,31,30,26], is that it is dependent on the radiofrequency offset.

Our previous contribution [33] also introduced a novel sequence, named S2hM (singlet to heteronuclear magnetization), that is capable of accomplishing singlet to heteronuclear order transfer under near magnetic equivalence conditions and, importantly, in an offset-independent manner.

In this paper, using the single transition operator formalism, we elucidate the theory behind S2hM, stressing the robustness of the method to RF offset mismatches and radiofrequency field inhomogeneities. Despite the apparent similarities with S2M (the sequence developed to convert singlet order into longitudinal magnetization in homonuclear systems [11,12,24]), this method runs

* Corresponding author.

E-mail address: g.pileio@soton.ac.uk (G. Pileio).

entirely on the heteronuclear channel and performs a different quantum mechanical evolution in the spin space detailed below. In the following analysis, we assume a near magnetic equivalent three-spin-1/2 system comprising two chemically equivalent spins-1/2 coupled to a third spin-1/2. The symmetry of the system is broken by a difference in the heteronuclear J couplings.

In the experimental session, we generate thermally polarised singlet order via the M2S sequence [24], described in detail in Section 3.2.

This paper deals with a 3 spin-1/2 system sketched in Fig. 1. Two spin-1/2 of the same kind (I-spins) make up a singlet pair; these two spins are assumed chemically equivalent, i.e. they have the same chemical shift frequency. A third spin is coupled to the singlet pair but belongs to a different nuclear species (S-spin). The scalar coupling frequency between the two spins in the singlet pair, $|J_{12}|$ is assumed bigger than the absolute difference between the two heteronuclear couplings, $|J_{13} - J_{23}|$: the two I-spins form a spin system that is classified as chemically-equivalent but

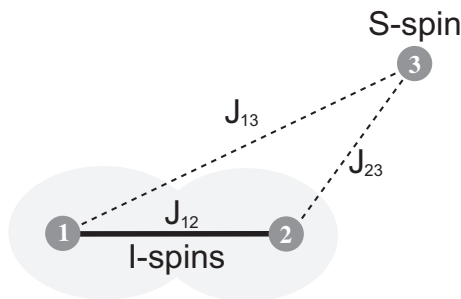


Fig. 1. A three-spin system formed by two chemically equivalent homonuclear spins (1 and 2), and a heteronuclear spin (3). The system is assumed in near equivalence regime, i.e. for $|J_{13} - J_{23}| < J_{12}$ with $J_{13} \neq J_{23}$.

magnetically-inequivalent [34]. A difference between heteronuclear scalar couplings is a condition to promote polarization transfer from singlet order.

2. Pulse sequence

The scheme for the storage of polarisation as singlet order and the subsequent detection through a heteronucleus is reported in Fig. 2. The core of the pulse sequence is the S2hM block which converts the singlet order of I-spins into transverse order of the S-spin. When compared to an S2M sequence [11,12,35,24], S2hM shows the following features: the sequence is run entirely on the heteronuclear channel and the length of the echo train is different, reflecting different spin dynamics.

The optimal values for the sequence parameters, under the assumed near magnetic equivalence regime, are:

$$\tau = \pi / \left(2\sqrt{(\omega_j^{12})^2 + (\omega_j^\Delta)^2} \right)$$

$$n = \text{round} \left[\pi / \left(4\text{ArcTan}(\omega_j^\Delta / \omega_j^{12}) \right) \right]. \quad (1)$$

where ω_j^{12} and ω_j^Δ are the homonuclear and heteronuclear imbalance in J couplings respectively, introduced later in Eq. (3). To generate the singlet order we used a modified version of the M2S pulse sequence (a variant of the M2S sequence for two-spins-1/2, described in Ref. [11,12,24] and of the one used for four-spins-1/2, presented in Ref. [13]) where the echo delay and the number of echoes have been adjusted to τ (same as in S2hM), $n_1 = 2n$ and $n_2 = n$, following the theory described below. These modifications are necessary because the I-spins are chemically-equivalent. The M2S block is followed by a T_{00} -filter [12,24] that suppresses all NMR signals not passing through I-spin singlet order. An optional storage delay, τ_{st} , follows and can be made variable

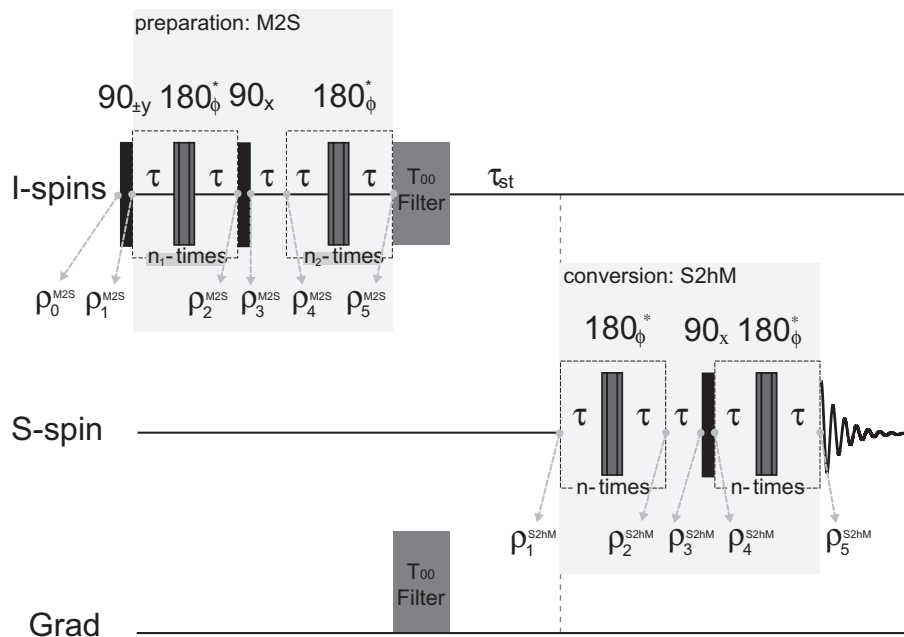


Fig. 2. Pulse sequence to prepare singlet order (M2S) and convert it into heteronuclear magnetisation (S2hM). The conversion block, S2hM is the core of the paper. The T_{00} block filters out any signals not passing through I-spins singlet order [12,24]. The * indicates that the 180 degrees pulse is a 90y180x90y composite pulse whose overall phase has been cycled as $\phi = \{x, x, y, y, y, x, x, y, y, y, x, x, y, y, y, x, x, x, y, y, x\}$ during the n-repetitions of the echo. The state of the system at the point i in the pulse sequence is described by the density operator ρ_i . $\tau = \pi / \left(2\sqrt{(\omega_j^{12})^2 + (\omega_j^\Delta)^2} \right)$, $n_1 = \text{round} \left[\pi / \left(2\text{ArcTan}(\omega_j^\Delta / \omega_j^{12}) \right) \right]$, $n_2 = n_1/2$ and $n = n_2$ (see Eq. (3)). The time interval τ_{st} has been introduced as a singlet storage delay with the intent of measuring the singlet decay rate via detection on the heteronucleus.

with the purpose of measuring the singlet order decay time, T_S through detection on the heteronuclear channel.

As demonstrated below, the overall effect of the method in Fig. 2 is to convert longitudinal order of the I-spins into singlet order of the same spins (M2S) and then convert this latter into transverse order of the S-spin (S2hM).

3. Theory

3.1. Spin Hamiltonian

The coherent liquid-state nuclear spin Hamiltonian expressed in the rotating frame of both I and S spins is:

$$[H]_{\mathbb{S}\mathbb{T}\mathbb{Z}} = \begin{matrix} & \textcircled{1} & \textcircled{2} & \textcircled{3} & \textcircled{4} & \textcircled{5} & \textcircled{6} & \textcircled{7} & \textcircled{8} \\ \textcircled{1} & \left(\begin{array}{cccccccc} -\frac{3\omega_J^{12}}{4} & \frac{\omega_J^\Delta}{2} & 0 & 0 & 0 & 0 & 0 & 0 & 0 \\ \frac{\omega_J^\Delta}{2} & \frac{\omega_J^{12}}{4} & 0 & 0 & 0 & 0 & 0 & 0 & 0 \\ 0 & 0 & -\frac{3\omega_J^{12}}{4} & -\frac{\omega_J^\Delta}{2} & 0 & 0 & 0 & 0 & 0 \\ 0 & 0 & -\frac{\omega_J^\Delta}{2} & \frac{\omega_J^{12}}{4} & 0 & 0 & 0 & 0 & 0 \\ 0 & 0 & 0 & 0 & \frac{1}{4}(\omega_J^{12} + 2\omega_J^\Sigma) & 0 & 0 & 0 & 0 \\ 0 & 0 & 0 & 0 & 0 & \frac{1}{4}(\omega_J^{12} - 2\omega_J^\Sigma) & 0 & 0 & 0 \\ 0 & 0 & 0 & 0 & 0 & 0 & \frac{1}{4}(\omega_J^{12} - 2\omega_J^\Sigma) & 0 & 0 \\ 0 & 0 & 0 & 0 & 0 & 0 & 0 & \frac{1}{4}(\omega_J^{12} + 2\omega_J^\Sigma) & 0 \end{array} \right) & & & & & & & & \end{matrix} \quad (8)$$

$$H = \omega_J^{12} \mathbf{I}_1 \cdot \mathbf{I}_2 + (\omega_J^\Sigma + \omega_J^\Delta) \mathbf{I}_{1z} \mathbf{I}_{3z} + (\omega_J^\Sigma - \omega_J^\Delta) \mathbf{I}_{2z} \mathbf{I}_{3z} \quad (2)$$

with

$$\begin{aligned} \omega_J^{12} &= 2\pi J_{12} \\ \omega_J^\Sigma &= \pi(J_{13} + J_{23}) \\ \omega_J^\Delta &= \pi(J_{13} - J_{23}) \end{aligned} \quad (3)$$

and where chemical shifts terms have been ignored implying that either the two I-spins are chemically equivalent or that any inequivalence is small enough to be ignored.

3.2. I-spins M2S

In this subsection we describe the singlet order preparation step (M2S, Fig. 2).

3.2.1. Basis functions

To define a convenient basis for the spin system above we start defining the singlet and triplet sub-basis of spin-1 and spin-2 as:

$$\mathbb{S}\mathbb{T}^{12} = \left\{ |S_0^{12}\rangle, |T_0^{12}\rangle, |T_1^{12}\rangle, |T_{-1}^{12}\rangle \right\} \quad (4)$$

with

$$\begin{aligned} |S_0^{12}\rangle &= \frac{1}{\sqrt{2}}(|\alpha_1\beta_2\rangle - |\beta_1\alpha_2\rangle) \\ |T_0^{12}\rangle &= \frac{1}{\sqrt{2}}(|\alpha_1\beta_2\rangle + |\beta_1\alpha_2\rangle) \\ |T_1^{12}\rangle &= |\alpha_1\alpha_2\rangle \\ |T_{-1}^{12}\rangle &= |\beta_1\beta_2\rangle \end{aligned} \quad (5)$$

and the Zeeman sub-basis for spin-3 as:

$$\mathbb{Z}^3 = \{\alpha_3, \beta_3\} \quad (6)$$

We then take the direct product between the two sub-bases to obtain:

$$\begin{aligned} \mathbb{S}\mathbb{T}\mathbb{Z} &= \mathbb{S}\mathbb{T}^{12} \otimes \mathbb{Z}^3 \\ &= \left\{ |S_0^{12}\alpha_3\rangle, |T_0^{12}\alpha_3\rangle, |S_0^{12}\beta_3\rangle, |T_0^{12}\beta_3\rangle, |T_1^{12}\alpha_3\rangle, |T_{-1}^{12}\alpha_3\rangle, |T_1^{12}\beta_3\rangle, |T_{-1}^{12}\beta_3\rangle \right\} \end{aligned} \quad (7)$$

with the basis re-arranged for convenience.

3.2.2. Spin Hamiltonian in single-transition spin operator formalism

The matrix representation of the Hamiltonian in Eq. (2) expressed in the $\mathbb{S}\mathbb{T}\mathbb{Z}$ basis is:

and therefore the Hamiltonian can be decomposed into the direct sum of 4 orthogonal bi-dimensional subspaces according to:

$$H = H^{12} \oplus H^{34} \oplus H^{56} \oplus H^{78}, \quad (9)$$

with:

$$\begin{aligned} H^{12} &= -\omega_J^{12} \mathbf{I}_z^{12} + \omega_J^\Delta \mathbf{I}_x^{12} - \frac{\omega_J^{12}}{4} \mathbf{1}^{12} \\ H^{34} &= -\omega_J^{12} \mathbf{I}_z^{34} - \omega_J^\Delta \mathbf{I}_x^{34} - \frac{\omega_J^{12}}{4} \mathbf{1}^{34} \\ H^{56} &= \omega_J^\Sigma \mathbf{I}_z^{56} + \frac{\omega_J^{12}}{4} \mathbf{1}^{56} \\ H^{78} &= -\omega_J^\Sigma \mathbf{I}_z^{78} + \frac{\omega_J^{12}}{4} \mathbf{1}^{78} \end{aligned} \quad (10)$$

where the superscript rs ($r, s \in \{1, 2, \dots, 8\}$) indicates the subspace spanned by the r -th and s -th functions in the $\mathbb{S}\mathbb{T}\mathbb{Z}$ basis and \mathbf{I}_k^{rs} is the single-transition spin operator [36,37] along the k -axis for the rs subspace defined as:

$$\begin{aligned} \mathbf{I}_x^{rs} &= \frac{1}{2}(|r\rangle\langle s| + |s\rangle\langle r|) \\ \mathbf{I}_y^{rs} &= \frac{1}{2i}(|r\rangle\langle s| - |s\rangle\langle r|) \\ \mathbf{I}_z^{rs} &= \frac{1}{2}(|r\rangle\langle r| - |s\rangle\langle s|) \\ \mathbf{1}^{rs} &= (|r\rangle\langle r| + |s\rangle\langle s|) \end{aligned} \quad (11)$$

that satisfies the following commutation rules:

$$[\mathbf{I}_x^\alpha, \mathbf{I}_y^\beta] = \begin{cases} 0 & \text{if } \alpha \neq \beta \\ -i\mathbf{I}_z^\alpha & \text{(cyclic) if } \alpha = \beta \end{cases} \quad (12)$$

Furthermore, by introducing:

$$\theta = \arctan\left(\frac{\omega_J^\Delta}{\omega_J^{12}}\right) \quad (13)$$

$$\omega_e = \sqrt{(\omega_J^{12})^2 + (\omega_J^\Delta)^2} \quad (14)$$

the Hamiltonian operators for the subspaces spanned by kets 1, 2 and 3, 4 can be rearranged as:

$$\begin{aligned} H^{12} &= \omega_e \widehat{R}_y^{12}(\pi - \theta) \mathbf{I}_z^{12} - \frac{\omega_J^{12}}{4} \mathbf{1}^{12} \\ H^{34} &= \omega_e \widehat{R}_y^{34}(\pi + \theta) \mathbf{I}_z^{34} - \frac{\omega_J^{12}}{4} \mathbf{1}^{34} \end{aligned} \quad (15)$$

with $\widehat{R}_k^r(\theta)$ being the rotation superoperator that rotates an operator by the angle θ about the k-axis of the subspace spanned by kets r and s .

The total Hamiltonian of Eq. (2) in this single transition spin operator formalism is finally given by:

$$\begin{aligned} H &= \omega_e \left[\widehat{R}_y^{12}(\pi - \theta) \mathbf{I}_z^{12} + \widehat{R}_y^{34}(\pi + \theta) \mathbf{I}_z^{34} \right] + \omega_J^\Sigma \left(\mathbf{I}_z^{56} - \mathbf{I}_z^{78} \right) \\ &\quad - \frac{\omega_J^{12}}{4} \left(\mathbf{1}^{12} + \mathbf{1}^{34} - \mathbf{1}^{56} - \mathbf{1}^{78} \right) \end{aligned} \quad (16)$$

3.2.3. Evolution in single-transition spin operator formalism

Because the Hamiltonian in Eq. (16) appears as a direct sum of Hamiltonians defined within independent subspaces, the associated propagator results as the product of 4 propagators acting, independently, in each subspace, i.e.:

$$\widehat{U}(\tau) = \widehat{U}^{12}(\tau) \widehat{U}^{34}(\tau) \widehat{U}^{56}(\tau) \widehat{U}^{78}(\tau) \quad (17)$$

with

$$\widehat{U}^{rs}(\tau) = e^{-iH^{rs}\tau} \quad (18)$$

The propagator in each subspace is written as:

$$\begin{aligned} \widehat{U}^{12}(\tau) &= \widehat{R}_y^{12}(\pi - \theta) \widehat{R}_z^{12}(\omega_e \tau) \widehat{R}_y^{12}(-\pi + \theta) \widehat{\Phi}^{12} \left(-\frac{\omega_J^{12}}{4} \tau \right) \\ \widehat{U}^{34}(\tau) &= \widehat{R}_y^{34}(\pi + \theta) \widehat{R}_z^{34}(\omega_e \tau) \widehat{R}_y^{34}(-\pi - \theta) \widehat{\Phi}^{34} \left(-\frac{\omega_J^{12}}{4} \tau \right) \\ \widehat{U}^{56}(\tau) &= \widehat{R}_z^{56}(\omega_J^\Sigma \tau) \widehat{\Phi}^{56} \left(\frac{\omega_J^{12}}{4} \tau \right) \\ \widehat{U}^{78}(\tau) &= \widehat{R}_z^{78}(-\omega_J^\Sigma \tau) \widehat{\Phi}^{78} \left(\frac{\omega_J^{12}}{4} \tau \right) \end{aligned} \quad (19)$$

with

$$\widehat{\Phi}^{rs}(\phi) = e^{-i\phi \mathbf{I}^{rs}} \quad (20)$$

All $\widehat{\Phi}^{rs}(\phi)$ terms and the propagators $\widehat{U}^{56}(\tau)$ and $\widehat{U}^{78}(\tau)$ contribute only to the signal phase and can be ignored in the following, for the sake of simplicity. The relevant propagator for the free evolution during a time interval τ and for $\theta \ll 1$ can then be approximated by [24]:

$$\begin{aligned} \widehat{U}_{free}^{M2S}(\tau) &= \widehat{R}_y^{12}(\pi - \theta) \widehat{R}_z^{12}(\omega_e \tau) \widehat{R}_y^{12}(-\pi + \theta) \widehat{R}_y^{34}(\pi + \theta) \widehat{R}_z^{34}(\omega_e \tau) \widehat{R}_y^{34}(-\pi - \theta) \\ &\approx \widehat{R}_z^{12}(\omega_e \tau) \widehat{R}_z^{34}(\omega_e \tau) \end{aligned} \quad (21)$$

and, for $\tau = \pi/(2\omega_e)$ reduces to:

$$\widehat{U}_{free}^{M2S} \left(\frac{\pi}{2\omega_e} \right) \approx \widehat{R}_z^{12} \left(\frac{\pi}{2} \right) \widehat{R}_z^{34} \left(\frac{\pi}{2} \right) \quad (22)$$

Within the same approximations, the propagator that describes the evolution during an echo block of the kind $\tau - 180_x - \tau$ with $\tau = \pi/(2\omega_e)$ can be approximated as [24]:

$$\widehat{U}_{echo}^{M2S} \left(\frac{\pi}{2\omega_e} \right) \approx \widehat{R}_x^{12}(2\theta) \widehat{R}_x^{34}(-2\theta) \quad (23)$$

The approximation $\theta \ll 1$ is valid under the assumption of near magnetic equivalence (see Eq. (13)).

3.2.4. M2S pulse sequence description

The initial thermal equilibrium state of the I-spins is represented by the density operator [33]:

$$\rho_0^{M2S} = \frac{1}{8} \mathbf{1} + \frac{1}{4} p_{Iz}^{eq} (\mathbf{I}_{1z} + \mathbf{I}_{2z}) \quad (24)$$

with

$$p_{Iz}^{eq} \approx \frac{\hbar \gamma_I B_0}{2k_B T} \quad (25)$$

where \hbar is the reduced Plank constant, k_B is the Boltzmann constant, T is the temperature, B_0 is the static magnetic field and γ_I is the gyromagnetic ratio of I-spins (valid at high temperature regimes, i.e. for $k_B T \gg |\hbar \gamma_I B_0|$). The unity operator does not participate to the evolution and is therefore ignored in all successive calculations. The first 90y radiofrequency pulse rotates the initial state by 90° about the y-axis to give:

$$\begin{aligned} \rho_1^{M2S} &= \frac{1}{4} p_{Iz}^{eq} (\mathbf{I}_{1x} + \mathbf{I}_{2x}) = \frac{1}{4\sqrt{2}} p_{Iz}^{eq} \left[(|T_1^{12} \alpha_3\rangle + |T_{-1}^{12} \alpha_3\rangle) \langle T_0^{12} \alpha_3| \right. \\ &\quad + (|T_1^{12} \beta_3\rangle + |T_{-1}^{12} \beta_3\rangle) \langle T_0^{12} \beta_3| + |T_0^{12} \alpha_3\rangle \left(\langle T_1^{12} \alpha_3| + \langle T_{-1}^{12} \alpha_3| \right) \\ &\quad \left. + |T_0^{12} \beta_3\rangle \left(\langle T_1^{12} \beta_3| + \langle T_{-1}^{12} \beta_3| \right) \right] \end{aligned} \quad (26)$$

Successively, a series of $n_1 = \frac{\pi}{2\theta}$ echo blocks of the form $\tau - 180_x - \tau$ with $\tau = \pi/(2\omega_e)$ is applied. The propagator for a single echo event, in the limit $\theta \ll 1$, is given in Eq. (23) and the total propagator after n_1 echoes becomes:

$$\left[\widehat{U}_{echo}^{M2S} \left(\frac{\pi}{2\omega_e} \right) \right]^{n_1} \approx \widehat{R}_x^{12}(\pi) \widehat{R}_x^{34}(-\pi) \quad (27)$$

This propagator acts by interchanging $|T_0^{12} \alpha_3\rangle$ with $-i|S_0^{12} \alpha_3\rangle$, $|T_0^{12} \beta_3\rangle$ with $i|S_0^{12} \beta_3\rangle$ while leaving all other functions unchanged. Accordingly, the density operator after this event becomes:

$$\begin{aligned} \rho_2^{M2S} &= \frac{i}{4\sqrt{2}} p_{Iz}^{eq} \left[(|T_1^{12} \alpha_3\rangle + |T_{-1}^{12} \alpha_3\rangle) \langle S_0^{12} \alpha_3| \right. \\ &\quad - (|T_1^{12} \beta_3\rangle + |T_{-1}^{12} \beta_3\rangle) \langle S_0^{12} \beta_3| + |S_0^{12} \alpha_3\rangle \left(\langle T_1^{12} \alpha_3| + \langle T_{-1}^{12} \alpha_3| \right) \\ &\quad \left. - |S_0^{12} \beta_3\rangle \left(\langle T_1^{12} \beta_3| + \langle T_{-1}^{12} \beta_3| \right) \right] \end{aligned} \quad (28)$$

The following 90x radiofrequency pulse rotates the actual density operator by 90° about the x-axis. It interchanges $(|T_1^{12} \alpha_3\rangle + |T_{-1}^{12} \alpha_3\rangle)$ with $-i\sqrt{2}|T_0^{12} \alpha_3\rangle$, $(|T_1^{12} \beta_3\rangle + |T_{-1}^{12} \beta_3\rangle)$ with $-i\sqrt{2}|T_0^{12} \beta_3\rangle$ leaving $|S_0^{12} \alpha_3\rangle$ and $|S_0^{12} \beta_3\rangle$ unaltered. The resulting density operator after this event is:

$$\begin{aligned} \rho_3^{M2S} &= \frac{1}{4} p_{Iz}^{eq} \left[|T_0^{12} \alpha_3\rangle \langle S_0^{12} \alpha_3| - |T_0^{12} \beta_3\rangle \langle S_0^{12} \beta_3| + |S_0^{12} \alpha_3\rangle \langle T_0^{12} \alpha_3| \right. \\ &\quad \left. - |S_0^{12} \beta_3\rangle \langle T_0^{12} \beta_3| \right] = \frac{1}{2} p_{Iz}^{eq} (\mathbf{I}_x^{12} - \mathbf{I}_x^{34}) \end{aligned} \quad (29)$$

Successively, the system is left to evolve under the internal Hamiltonian for the time interval $\tau = \pi/(2\omega_e)$. The related propagator is given in Eq. (22) and corresponds to a 90° rotation about the z-axis of the 1, 2 and 3, 4 sub-spaces that leads to:

$$\rho_4^{M2S} = \frac{1}{2} p_{Iz}^{eq} (\mathbf{I}_y^{12} - \mathbf{I}_y^{34}) \quad (30)$$

Finally, a series of $n_2 = \frac{\pi}{4\theta}$ echo blocks of the form $\tau - 180_x - \tau$ with $\tau = \pi/(2\omega_e)$ is applied, corresponding to a rotation of 90° about the x-axis of the 1, 2 sub-space and of -90° about the x-axis of the 3, 4 sub-space (see Eqs. (23) and (27)) and leading to:

$$\rho_5^{M2S} = \frac{1}{2} p_{Iz}^{eq} (\mathbf{I}_z^{12} + \mathbf{I}_z^{34}) = -\frac{1}{4} p_{Iz}^{eq} (\mathbf{I}_1^+ \mathbf{I}_2^- + \mathbf{I}_1^- \mathbf{I}_2^+) \quad (31)$$

corresponding to a population imbalance of the kind:

$$\rho_5^{M2S} = -\frac{1}{4} p_{lz}^{eq} \left(|S_0^{12} \alpha_3\rangle \langle S_0^{12} \alpha_3| - |T_0^{12} \alpha_3\rangle \langle T_0^{12} \alpha_3| + |S_0^{12} \beta_3\rangle \langle S_0^{12} \beta_3| - |T_0^{12} \beta_3\rangle \langle T_0^{12} \beta_3| \right) \quad (32)$$

The operator amplitude $\langle A \rightarrow B \rangle$ given by:

$$\langle A \rightarrow B \rangle = \frac{\langle B|A \rangle}{\langle B|B \rangle} \quad (33)$$

with

$$\langle B|A \rangle = \text{Tr}\{B^\dagger A\} \quad (34)$$

extracts the coefficient of the operator B contained in operator A [33]. The Zeeman polarisation of spins 1 and 2 along the x-axis (corresponding to the polarisation level operator after the first 90° pulse in the M2S pulse sequence) is therefore derived as:

$$p_x = \langle \rho \rightarrow P_{1x} + P_{2x} \rangle \quad (35)$$

with

$$P_{jx} = 2^{1-N} \mathbf{I}_j^x \quad (36)$$

being the Zeeman polarisation level operator along the x-axis. The singlet polarisation level operator for a spin pair j, k in a spin system made by N spins is given by:

$$P_s^{j,k} = -2^{2-N} \mathbf{I}_j \cdot \mathbf{I}_k \quad (37)$$

Therefore, the operator amplitude:

$$p_s^{j,k} = \langle \rho \rightarrow P_s^{j,k} \rangle \quad (38)$$

extracts the amount of singlet polarisation, $p_s^{j,k}$, contained in the generic density operator ρ . For the three spin system discussed in this paper the singlet polarisation level operator is therefore:

$$P_s^{1,2} = -\frac{1}{2} \mathbf{I}_1 \cdot \mathbf{I}_2 \quad (39)$$

and we can use Eq. (38) to figure out the theoretical efficiency of the I-spins M2S as:

$$p_s^{1,2}(M2S) = \langle \rho_5^{M2S} \rightarrow P_s^{1,2} \rangle = \frac{2}{3} p_{lz}^{eq} \quad (40)$$

The value of 2/3 coincide with the maximum transformation amplitude for the conversion of Zeeman order into singlet order under unitary transformations [24]. Fig. 3 shows the trajectories of $P_{1x} + P_{2x}$ (gray) and $P_s^{1,2}$ (black) versus time for the M2S pulse sequence with $\tau = 64$ ms, $n_1 = 8$ and $n_2 = 4$.

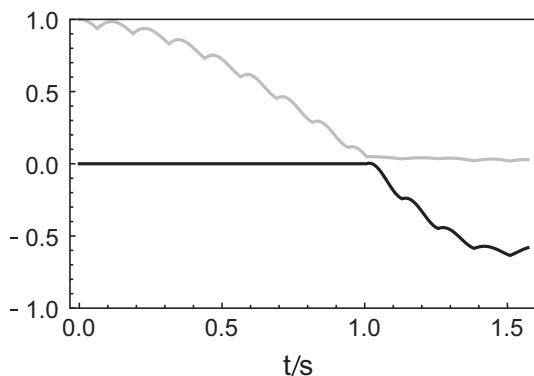


Fig. 3. Trajectories of the polarization level operators $P_{1x} + P_{2x}$ (gray) and $P_s^{1,2}$ (black) versus time for the M2S pulse sequence with $\tau = 64$ ms, $n_1 = 8$ and $n_2 = 4$.

3.3. S-spin S2hM

In this subsection we describe the S2hM pulse sequence for the conversion of singlet order into heteronuclear magnetisation (S2hM, Fig. 2).

3.3.1. Basis functions

When discussing the S2hM sequence it is convenient to use a slightly different basis than the one used above for the M2S block. Following the convention adopted in Ref. [34], we use the basis built as the direct product between the $\mathbb{S}\mathbb{T}^{12}$ basis of Eq. (4) and the eigenbasis of the operator \mathbf{I}_{3x} written as:

$$\mathbb{X}^3 = \left\{ \left| \Delta_{\alpha\beta}^3 \right\rangle, \left| \Sigma_{\alpha\beta}^3 \right\rangle \right\} \quad (41)$$

with

$$\begin{aligned} \left| \Delta_{\alpha\beta}^3 \right\rangle &= \frac{1}{\sqrt{2}} (|\beta_3\rangle - |\alpha_3\rangle) \\ \left| \Sigma_{\alpha\beta}^3 \right\rangle &= \frac{1}{\sqrt{2}} (|\beta_3\rangle + |\alpha_3\rangle) \end{aligned} \quad (42)$$

The resulting $\mathbb{S}\mathbb{T}\mathbb{X}$ basis is therefore:

$$\begin{aligned} \mathbb{S}\mathbb{T}\mathbb{X} &= \mathbb{S}\mathbb{T}^{12} \otimes \mathbb{X}^3 \\ &= \left\{ \begin{array}{l} \left| S_0^{12} \Delta_{\alpha\beta}^3 \right\rangle, \left| T_0^{12} \Sigma_{\alpha\beta}^3 \right\rangle, \left| T_0^{12} \Delta_{\alpha\beta}^3 \right\rangle, \left| S_0^{12} \Sigma_{\alpha\beta}^3 \right\rangle, \left| T_1^{12} \Delta_{\alpha\beta}^3 \right\rangle, \left| T_1^{12} \Sigma_{\alpha\beta}^3 \right\rangle, \\ \left| T_{-1}^{12} \Delta_{\alpha\beta}^3 \right\rangle, \left| T_{-1}^{12} \Sigma_{\alpha\beta}^3 \right\rangle \end{array} \right\} \end{aligned} \quad (43)$$

where the basis functions have been re-arranged for convenience.

3.3.2. Spin Hamiltonian in single-transition spin operator formalism

The matrix representation of the Hamiltonian in Eq. (2) expressed in the $\mathbb{S}\mathbb{T}\mathbb{X}$ basis becomes:

$$[H]_{\mathbb{S}\mathbb{T}\mathbb{X}} = \begin{array}{c} \begin{array}{cccccccc} \textcircled{1} & \textcircled{2} & \textcircled{3} & \textcircled{4} & \textcircled{5} & \textcircled{6} & \textcircled{7} & \textcircled{8} \end{array} \\ \begin{array}{c} \textcircled{1} \\ \textcircled{2} \\ \textcircled{3} \\ \textcircled{4} \\ \textcircled{5} \\ \textcircled{6} \\ \textcircled{7} \\ \textcircled{8} \end{array} \left(\begin{array}{cccccccc} -\frac{3\omega_j^{12}}{4} & \frac{\omega_j^\Delta}{2} & 0 & 0 & 0 & 0 & 0 & 0 \\ \frac{\omega_j^\Delta}{2} & \frac{\omega_j^{12}}{4} & 0 & 0 & 0 & 0 & 0 & 0 \\ 0 & 0 & \frac{\omega_j^{12}}{4} & \frac{\omega_j^\Delta}{2} & 0 & 0 & 0 & 0 \\ 0 & 0 & \frac{\omega_j^\Delta}{2} & -\frac{3\omega_j^{12}}{4} & 0 & 0 & 0 & 0 \\ 0 & 0 & 0 & 0 & \frac{\omega_j^{12}}{4} & \frac{\omega_j^\Sigma}{2} & 0 & 0 \\ 0 & 0 & 0 & 0 & \frac{\omega_j^\Sigma}{2} & \frac{\omega_j^{12}}{4} & 0 & 0 \\ 0 & 0 & 0 & 0 & 0 & 0 & \frac{\omega_j^{12}}{4} & -\frac{\omega_j^\Sigma}{2} \\ 0 & 0 & 0 & 0 & 0 & 0 & -\frac{\omega_j^\Sigma}{2} & \frac{\omega_j^{12}}{4} \end{array} \right) \end{array} \quad (44)$$

and therefore the Hamiltonian can be decomposed in the direct sum of 4 orthogonal bidimensional subspaces according to:

$$H = H^{12} \oplus H^{34} \oplus H^{56} \oplus H^{78}, \quad (45)$$

with:

$$\begin{aligned} H^{12} &= -\omega_j^{12} \mathbf{I}_z^{12} + \omega_j^\Delta \mathbf{I}_x^{12} - \frac{\omega_j^{12}}{4} \mathbf{1}^{12} \\ H^{34} &= \omega_j^{12} \mathbf{I}_z^{34} + \omega_j^\Delta \mathbf{I}_x^{34} - \frac{\omega_j^{12}}{4} \mathbf{1}^{34} \\ H^{56} &= \omega_j^\Sigma \mathbf{I}_x^{56} + \frac{\omega_j^{12}}{4} \mathbf{1}^{56} \\ H^{78} &= -\omega_j^\Sigma \mathbf{I}_x^{78} + \frac{\omega_j^{12}}{4} \mathbf{1}^{78} \end{aligned} \quad (46)$$

Using the same definitions for θ and ω_e given in Eq. (13) the Hamiltonians for the subspaces spanned by kets 1, 2 and 3, 4 can be rearranged as:

$$H^{12} = \omega_e \widehat{R}_y^{12}(\pi - \theta) \mathbf{I}_z^{12} - \frac{\omega_J^{12}}{4} \mathbf{1}^{12} = -\omega_e \widehat{R}_y^{12}(-\theta) \mathbf{I}_z^{12} - \frac{\omega_J^{12}}{4} \mathbf{1}^{12}$$

$$H^{34} = \omega_e \widehat{R}_y^{34}(\theta) \mathbf{I}_z^{34} - \frac{\omega_J^{12}}{4} \mathbf{1}^{34} \quad (47)$$

and the total Hamiltonian of Eq. (2) in this new basis and within the single transition spin operator formalism is finally given by:

$$H = \omega_e \left[\widehat{R}_y^{34}(\theta) \mathbf{I}_z^{34} - \widehat{R}_y^{12}(-\theta) \mathbf{I}_z^{12} \right] + \omega_J^\Sigma \left(\mathbf{I}_x^{56} - \mathbf{I}_x^{78} \right) + \frac{\omega_J^{12}}{4} \left(\mathbf{1}^{56} + \mathbf{1}^{78} - \mathbf{1}^{12} - \mathbf{1}^{34} \right) \quad (48)$$

3.3.3. Evolution in single-transition spin operator formalism

As above, the evolution under the Hamiltonian in Eq. (48) during the time interval τ can be expressed as the product of the evolution in the 4 individual subspaces:

$$\widehat{U}(\tau) = \widehat{U}^{12}(\tau) \widehat{U}^{34}(\tau) \widehat{U}^{56}(\tau) \widehat{U}^{78}(\tau) \quad (49)$$

with:

$$\widehat{U}^{12}(\tau) = \widehat{R}_y^{12}(-\theta) \widehat{R}_z^{12}(-\omega_e \tau) \widehat{R}_y^{12}(\theta) \widehat{\Phi}^{12} \left(-\frac{\omega_J^{12}}{4} \tau \right)$$

$$\widehat{U}^{34}(\tau) = \widehat{R}_y^{34}(\theta) \widehat{R}_z^{34}(\omega_e \tau) \widehat{R}_y^{34}(-\theta) \widehat{\Phi}^{34} \left(-\frac{\omega_J^{12}}{4} \tau \right)$$

$$\widehat{U}^{56}(\tau) = \widehat{R}_x^{56}(\omega_J^\Sigma \tau) \widehat{\Phi}^{56} \left(\frac{\omega_J^{12}}{4} \tau \right)$$

$$\widehat{U}^{78}(\tau) = \widehat{R}_x^{78}(-\omega_J^\Sigma \tau) \widehat{\Phi}^{78} \left(\frac{\omega_J^{12}}{4} \tau \right) \quad (50)$$

The propagators $\widehat{U}^{56}(\tau)$ and $\widehat{U}^{78}(\tau)$ can be ignored since this sequence operates on singlet order which is confined within the subspaces spanned by the spin functions 1, 2 and 3, 4 (see Eq. (31)). The superoperators $\widehat{\Phi}^{rs}(\phi)$ can also be ignored for the sake of simplicity since they only contribute to the phase of the signal. The final form of the propagator for the free evolution during a time interval τ and for $\theta \ll 1$ can therefore be approximated as [24]:

$$\widehat{U}_{free}^{S2hM}(\tau) = \widehat{R}_y^{12}(-\theta) \widehat{R}_z^{12}(-\omega_e \tau) \widehat{R}_y^{12}(\theta) \widehat{R}_y^{34}(\theta) \widehat{R}_z^{34}(\omega_e \tau) \widehat{R}_y^{34}(-\theta) \approx \widehat{R}_z^{12}(-\omega_e \tau) \widehat{R}_z^{34}(\omega_e \tau) \quad (51)$$

and, for $\tau = \pi/(2\omega_e)$ reduces to:

$$\widehat{U}_{free}^{S2hM} \left(\frac{\pi}{2\omega_e} \right) \approx \widehat{R}_z^{12} \left(-\frac{\pi}{2} \right) \widehat{R}_z^{34} \left(\frac{\pi}{2} \right) \quad (52)$$

Within the same approximations, the evolution during a echo block $\tau - 180_x - \tau$ with $\tau = \pi/(2\omega_e)$ can be approximated [24] as:

$$\widehat{U}_{echo}^{S2hM} \left(\frac{\pi}{2\omega_e} \right) \approx \widehat{R}_x^{12}(2\theta) \widehat{R}_x^{34}(2\theta) \quad (53)$$

3.3.4. S2hM pulse sequence description

The starting density operator at the beginning of S2hM is generally equal to:

$$\rho_1^{S2hM} = -\frac{1}{2} p_3^I \mathbf{I}_1 \cdot \mathbf{I}_2 \quad (54)$$

with p_3^I representing the I-spin singlet polarisation which, in the case it is generated by the M2S sequence described above, is equal, at best, to $(2/3)p_{Iz}^{eq}$ (see Eq. (40)) and, in the case it is generated by an ideal reaction with pure parahydrogen, is 1 instead. This can be rewritten in terms of single transition spin operators as:

$$\rho_1^{S2hM} = \frac{1}{2} p_{Iz}^{eq} \left(\mathbf{I}_z^{12} - \mathbf{I}_z^{34} \right) + \frac{1}{8} p_{Iz}^{eq} \left(\mathbf{1}^{12} + \mathbf{1}^{34} - \mathbf{1}^{56} - \mathbf{1}^{78} \right) \quad (55)$$

with all unity operators neglected in the following as they do not participate in the evolution.

The first event in the S2hM is a series of $n = \frac{\pi}{4\theta}$ echo blocks of the form $\tau - 180_x - \tau$ with $\tau = \pi/(2\omega_e)$. The propagator for the event is derived from Eq. (53), in the limit $\theta \ll 1$, as:

$$\left[\widehat{U}_{echo}^{S2hM} \left(\frac{\pi}{2\omega_e} \right) \right]^n \approx \widehat{R}_x^{12} \left(\frac{\pi}{2} \right) \widehat{R}_x^{34} \left(\frac{\pi}{2} \right) \quad (56)$$

corresponding to a rotation of 90° about the x-axis of the 1, 2 and 3, 4 sub-spaces. The density operator after this event is:

$$\rho_2^{S2hM} = \frac{1}{2} p_{Iz}^{eq} \left(-\mathbf{I}_y^{12} + \mathbf{I}_y^{34} \right) \quad (57)$$

This density operator evolves for a time interval $\tau = \pi/(2\omega_e)$ under the propagator in Eq. (52) to become:

$$\rho_3^{S2hM} = \frac{1}{2} p_{Iz}^{eq} \left(-\mathbf{I}_x^{12} - \mathbf{I}_x^{34} \right) \quad (58)$$

The propagator for the successive 90_x pulse, written in this basis and within the single-transition operators formalism, is $\widehat{R}_z^{12}(-\pi/2) \widehat{R}_z^{34}(-\pi/2)$. When applied to ρ_3^{S2hM} it generates:

$$\rho_4^{S2hM} = \frac{1}{2} p_{Iz}^{eq} \left(\mathbf{I}_y^{12} + \mathbf{I}_y^{34} \right) \quad (59)$$

Finally, a second echo train of $n = \frac{\pi}{4\theta}$ blocks of the form $\tau - 180_x - \tau$ with $\tau = \pi/(2\omega_e)$ produces a final rotation of 90° about the x-axis of the 1, 2 and 3, 4 sub-spaces (Eq. (56)) yielding:

$$\rho_5^{S2hM} = \frac{1}{2} p_{Iz}^{eq} \left(\mathbf{I}_z^{12} + \mathbf{I}_z^{34} \right) = -\frac{1}{4} p_{Iz}^{eq} \left(\mathbf{I}_{3x} - 4\mathbf{I}_{1z}\mathbf{I}_{2z}\mathbf{I}_{3x} \right) \quad (60)$$

corresponding to a single peak centred at the chemical shift of the S-spin plus an out-of-phase term giving rise to an out-of-phase multiplet signal also centred at the chemical shift of the S-spin and spaced by ω_J^Σ . To extract the amount of transverse order contained into ρ_5^{S2hM} we use the same technique as above consisting in evaluating the following operator amplitude:

$$p_{3x}(S2hM) = \langle \rho_5^{S2hM} \rightarrow P_{3x} \rangle = -p_5^I \quad (61)$$

with

$$P_{3x} = 2^{1-N} \mathbf{I}_{3x} = \frac{1}{4} \mathbf{I}_{3x} \quad (62)$$

meaning that the transfer between singlet order of spin-1 and 2 into heteronuclear transverse magnetisation of spin-3 operated by a S2hM pulse sequence has a theoretical maximum efficiency of 1.

Fig. 4 shows the trajectories of $P_5^{1,2}$ (gray) and P_{3x} (black) versus time for the S2hM pulse sequence with $\tau = 64$ ms and $n = 4$.

3.4. Robustness

Fig. 5 shows the result of a numerical simulation aimed at calculating the amplitude of the singlet to heteronuclear polarization transfer implemented by the S2hM pulse sequence as a function of the ^{13}C frequency offset and considering a $\pm 10\%$ B_1 inhomogeneity. The simulation uses the parameters for 2,5-thiophenedicarboxylic acid reported in Fig. 6. The error on the B_1 offset is assumed to be systematic and equal on every cycle of the echo train. The conversion is particularly robust to frequency offset mismatch as opposed to SLIC and ADAPT [34] while more sensitive to B_1 inhomogeneities (Fig. 5a). However, the incidence of B_1 errors is removed by implementing composite 180° pulses (Fig. 5b).

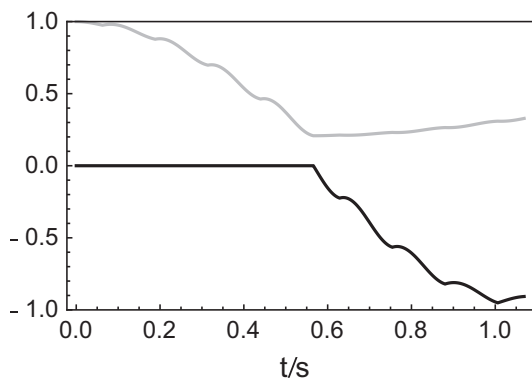


Fig. 4. Trajectories of the polarization level operators $P_s^{1,2}$ (gray) and P_{3x} (black) versus time for the S2hM pulse sequence with $\tau = 64$ ms and $n = 4$.

Table 1 reports the results of numerical simulations on a variety of chemical systems (typically used in parahydrogen experiments [26,34]) with the intent to compare S2hM with other singlet to heteronuclear order conversion methodologies. The table is meant to demonstrate that although the analysis of the S2hM pulse sequence presented above is done in the near equivalence limit, the method can still be applied outside this regime with good performances. Despite taking longer than other methods, S2hM achieves a significant polarization transfer under diverse conditions of magnetic equivalence. This flexibility, together with the robustness with respect to frequency offset mismatches and B_1 inhomogeneities, makes the method applicable in a variety of real systems.

4. Results and discussion

To test the methodology we used a sample of 2,5-thiophenedicarboxylic acid (Fig. 6) where the two protons on the thiophene ring make up the I-spins and the natural abundant carbonyl- ^{13}C spin (abundance $\sim 2\%$) is the S-spin. The compound was purchased from Sigma-Aldrich and used without further purification in a 0.4 M solution in DMSO- d_6 , degassed by N_2 -bubbling to remove dissolved oxygen. The molecule was chosen

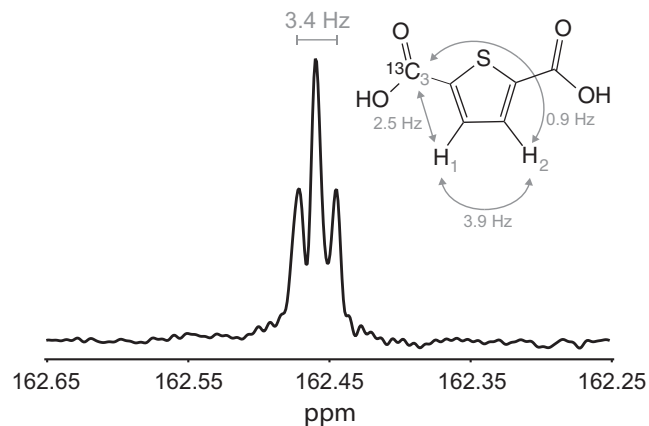


Fig. 6. Molecular structure (^{13}C -isotopomer) and ^{13}C NMR pulse-acquire spectrum of a 0.4 M sample of 2,5-thiophenedicarboxylic acid in DMSO- d_6 .

to stress some advantages of S2hM over the SLIC method: SLIC requires continuous irradiation for some hundreds of milliseconds at a nutation frequency that matches J_{12} , which for this systems corresponds to such a low power that the instrument is unable to supply with the required stability.

In near-magnetic-equivalence conditions, the single quantum ^1H and ^{13}C NMR spectra only contain information on the proton-proton coupling, $\omega_J^{12}/2\pi = 3.9$ Hz and the mean of the two heteronuclear couplings, $\omega_J^{\Sigma}/2\pi = 1.7$ Hz. The optimal values for τ , n_1 , n_2 and n (requiring individual values of the heteronuclear couplings) were experimentally determined by running a 90y-M2S- T_{00} filter-S2hM experiment (Fig. 2) at variable values of n with $n_1 = 2n$, $n_2 = n$ and τ fixed within a range of expected values (Fig. 7a shows the case $\tau = 63$ ms, black points) and, successively, fixing $n = 4$ (best value in the optimisation above) and varying τ to find its optimal value to be $\tau = 64$ ms (see Fig. 7b, black points). Using the analytical expressions for τ and n a value of $\omega_J^{\Delta}/2\pi = 0.8$ Hz is found. The individual value of the two heteronuclear couplings is then found by solving the system of equation $\omega_J^{\Delta}/2\pi = 0.8$ Hz and $\omega_J^{\Sigma}/2\pi = 1.7$ Hz giving $J_{13} = 2.5$ Hz and $J_{23} = 0.9$ Hz and $\theta = 11.6^\circ$ (see Eq. (13)).

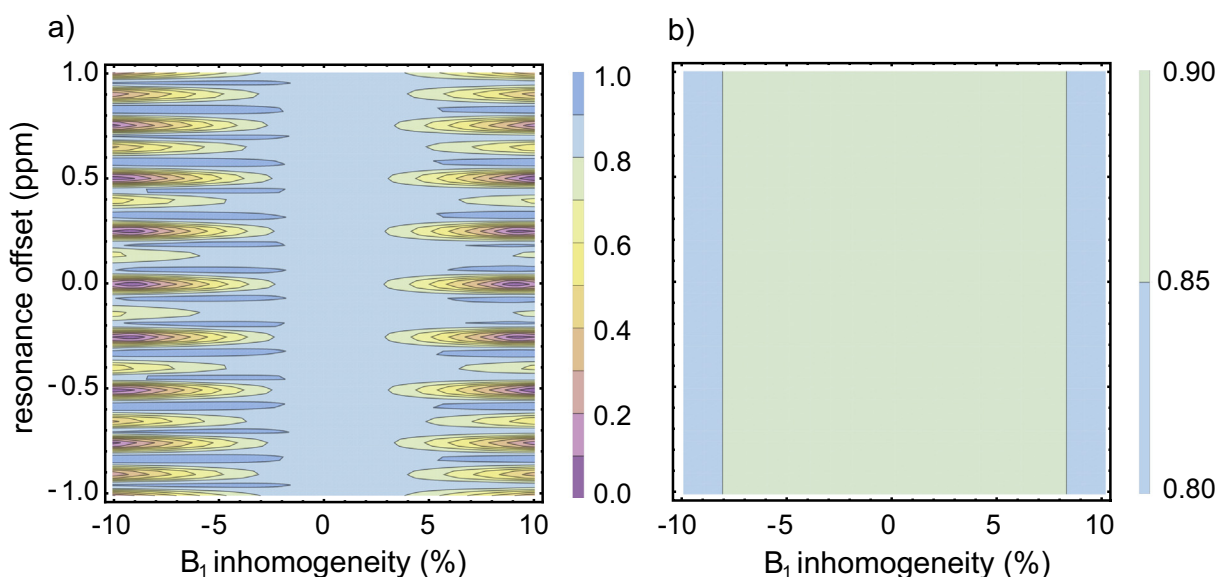


Fig. 5. Simulated conversion efficiency for the S2hM pulse sequence in Fig. 2 in the case of 2,5-thiophenedicarboxylic acid and plotted as a function of the resonance offset and pulse imperfection; (a) using a single hard 180° pulse in the echo trains and (b) using 180° pulses replaced by composite pulses of the kind 90y180x90y.

Table 1
Numerical simulations testing S2hM versus ADAPT, Goldman and Kadlecek pulse sequences. In particular the delays, number of loops, total duration, and achieved heteronuclear polarization (P) are indicated for TMVS (trimethylvinylsilane), TIFBU (trifluoro but-2-enoate), MEPA1/MEPA2 ([2-(2-Methoxyethoxy) ethyl]ethyl acrylate), SUC (succinic acid), HEP (hydroxyethylpropionate) and BIMAC (2-(2-methoxyethoxy) ethyl acrylate). The J coupling values in Hz taken from Ref. [26] and the angle θ , defined in Eq. (13), are indicated. The ADAPT parameters are taken from Ref. [34]. Timings: τ for S2hM, Δ_x for ADAPT_x, (t_1^x, t_2^x, \dots) for Kadlecek2x and (t_0^x, t_1^x, \dots) for Goldman. Loops: n for S2hM, m for ADAPT_x, n_3 for Kadlecek2b and (n_1, n_2, \dots) for Goldman.

Molecule	(J_{12}, J_{13}, J_{23}) (Hz)	θ ($^\circ$)	Sequence	Timings (ms)	Loops	Duration (ms)	P (%)
TMVS	(14.6,15.3,6.5)	16.8	S2hM	17.50	2	157.5	94
			ADAPT ₉₀	16.84	8	134.0	99
			Kadlecek2b	(22.42,36.45,32.79,8.42)	1	200.0	97
			Goldman	(32.79,18.10,30.76,32.79,32.79)	(2,6)	344.0	96
TIFBU	(12.5,8.4,0.8)	16.9	S2hM	20.00	2	180.0	93
			ADAPT ₉₀	19.67	8	157.4	98
			Kadlecek2b	(25.37,42.79,38.27,9.83)	1	232.0	97
			Goldman	(38.27,20.88,36.18,38.27,38.27)	(2,6)	401.5	96
MEPA1	(12.6,10.0,-1.8)	25.1	S2hM	15.00	3	195.0	94
			ADAPT ₄₅	9.81	8	78.5	98
			Kadlecek2a	(29.81,29.01)	-	117.6	100
			Goldman	(29.81)	-	196.3	96
MEPA2	(12.6,15.8,-2.5)	36.0	S2hM	13.50	2	121.5	90
			ADAPT ₉₀	17.00	4	68.0	92
			Kadlecek2a	(12.90,29.80)	-	85.5	100
			Goldman	(20.80,21.71,32.11)	-	74.6	95
SUC	(6.6,4.2,-6.6)	39.2	S2hM	25.00	2	225.0	91
			ADAPT ₉	3.77	22	83.0	93
			Kadlecek2a	(20.10,54.06)	-	148.0	100
			Goldman	(33.96,41.53,58.51)	-	134.0	98
HEP	(7.6,7.2,-5.6)	40.3	S2hM	22.00	9	198.0	91
			ADAPT ₁₂	4.75	15	71.2	95
			Kadlecek2a	(16.34,46.33)	-	125.0	100
			Goldman	(28.28,36.20,50.34)	-	114.8	99
BIMAC	(12.0,24.0,-2.5)	47.8	S2hM	13.00	9	481.0	82
			ADAPT ₉	2.1	18	37.8	100
			Kadlecek2a	(5.72,24.13)	-	59.7	100
			Goldman	(13.18,21.38,27.97)	-	62.5	100

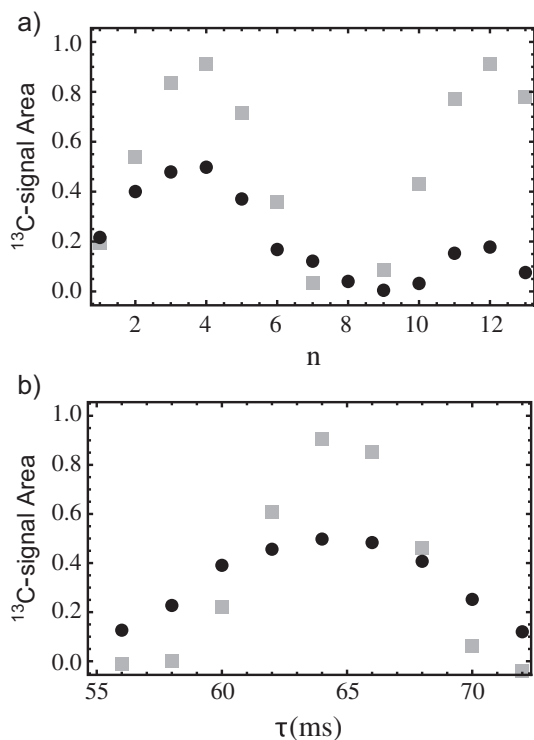


Fig. 7. Experimental (black circles) and simulated (grey squares) conversion efficiencies for the S2hM sequence plotted versus (a) n and (b) τ and obtained using the pulse sequence in Fig. 2. Experimental points have been scaled using the procedure reported in Ref. [33] and detailed in the Appendix.

Fig. 7 shows a plot of the area under the signal resulting after the pulse sequence in Fig. 2 versus (a) n and (b) τ . Experimental values are represented by black circles whereas simulated values are indicated by grey squares. Experimental points have been scaled using the procedure reported in Ref. [33] and detailed in Appendix. This procedure captures the individual efficiencies of M2S and S2hM. The experimental maximum transfer amplitude between the singlet order of spins-1 and 2 into heteronuclear transverse magnetisation of spin-3 is 0.5 (see Appendix). We have obtained similar experimental efficiencies on other systems with SLIC, Goldman and Kadlecek methods [33]. The simulated transfer amplitude for the same transformation is 0.9. The discrepancy between experiments and simulation is attributed to relaxation phenomena and experimental imperfections which where not

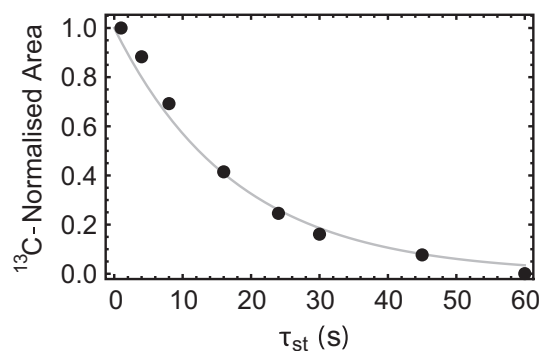


Fig. 8. Normalised ¹³C-signal area plotted versus τ_{st} as obtained using the pulse sequence in Fig. 2 for a 0.4 M sample of 2,5-thiophenedicarboxylic acid in DMSO- d_6 . The experimental points (black circles) are fitted to a single exponential function (solid grey curve) to yield the value of the singlet order decay time $T_S = 18.0 \pm 0.7$ s.

included into the simulations for the sake of simplicity. The experimental efficiency of the M2S on the I-spins was found to be 0.32 against a simulated value of 0.59.

In a final experiment, the pulse sequence in Fig. 2 was run with the optimal values of $\tau = 64$ ms, $n_1 = 8$, $n_2 = 4$ and $n = 4$ varying the time delay τ_{st} in order to measure the lifetime of the proton singlet order via detection on the carbon channel. The area under the NMR signal acquired on the ^{13}C -channel is plotted against τ_{st} in Fig. 8. The experimental points (black circles) were fitted to a single exponential to find the decay time constant of the singlet order $T_s = 18.0 \pm 0.7$ s. The values of the longitudinal order decay constant for ^1H and ^{13}C were measured using saturation recovery experiments and were found to be $T_1^H = 2.5 \pm 0.1$ s and $T_1^C = 5.0 \pm 0.1$ s, respectively.

5. Conclusion

In conclusion, we have presented and described a pulse sequence that accomplishes the task of converting two spins-1/2 homonuclear singlet order into heteronuclear magnetization. A theoretical description and experimental validation have been provided in the near equivalence regime. Only two parameters (n and τ) need to be optimized experimentally, and the sequence performs with significant conversion yields even far from magnetic equivalence. The robustness of the pulse sequence with respect to the frequency offset mismatches and field inhomogeneities makes S2hM a good candidate for widespread use within the PHIP arena. At high values of θ the sequence duration is longer than all other proposed methods which may be a drawback for some application.

Acknowledgement

This research was supported by EPSRC, Grant Nos. EP/M508147/1 and EP/N033558/1. We thank W. Hale and J. Alonso-Valdesueiro for experimental help and M.H. Levitt for reading the manuscript prior to submission. Most of the work in this article uses the *SpinDynamica* code for Wolfram Mathematica, programmed by Malcolm H. Levitt, with contributions from J. Rantaharju, A. Brinkmann, and S. Singha Roy, available at www.spindynamica.soton.ac.uk.

Appendix A

To measure the efficiency of the ^{13}C S2hM conversion step ($\langle P_S^I \xrightarrow{\text{S2hM}} P_z^S \rangle$), we employed the calibration scheme shown in Fig. A.9. A more detailed description can be found in Ref. [33].

We determine the efficiency of the conversion from I-spin Zeeman polarization (P_z^I) to S-spin Zeeman polarization (P_z^S) by calibrating the integrated signal amplitude from experiment 1 (a_A) against a pulse-acquire carbon signal in experiment 2 (a_B) (for experiments numbers refer to Fig. A.9).

$$a_A = f p_{Iz}^{\text{eq}} \langle P_z^I \xrightarrow{\text{M2S}} P_S^I \rangle \langle P_S^I \xrightarrow{\text{S2hM}} P_z^S \rangle \quad (\text{A.1})$$

$$a_B = f p_{Sz}^{\text{eq}} \quad (\text{A.2})$$

where f is an instrumental factor common to all experiments. From this we deduce

$$\langle P_z^I \xrightarrow{\text{M2S}} P_S^I \rangle \langle P_S^I \xrightarrow{\text{S2hM}} P_z^S \rangle = \frac{p_{Sz}^{\text{eq}} a_A}{p_{Iz}^{\text{eq}} a_B} = \frac{\gamma_S}{\gamma_I} \frac{a_A}{a_B} \quad (\text{A.3})$$

To eliminate the loss in efficiency due to the step $\langle P_z^I \xrightarrow{\text{M2S}} P_S^I \rangle$, we introduce experiments 3 and 4 (see Fig. A.9). The corresponding signal amplitudes are as follows:

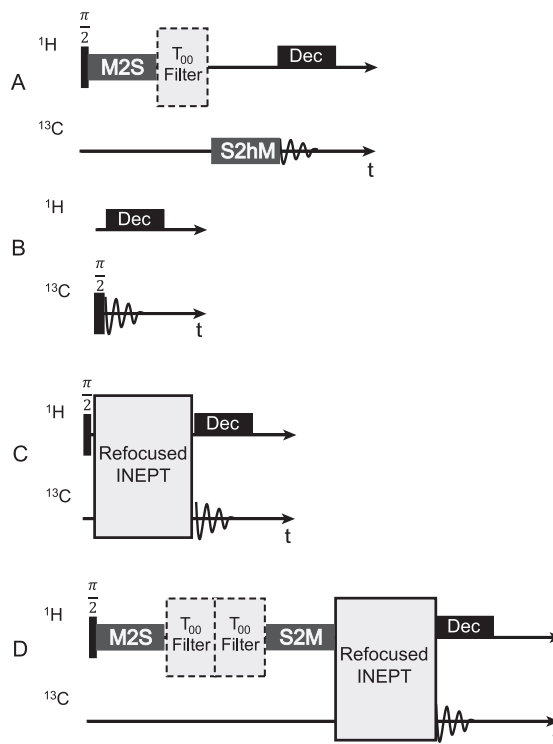


Fig. A.9. Pulse sequences for calibration of the conversion efficiency of the S2hM sequence.

$$a_C = f p_{Iz}^{\text{eq}} \langle P_z^I \xrightarrow{\text{INEPT}} P_z^S \rangle \quad (\text{A.4})$$

$$a_D = \frac{3}{2} f p_{Iz}^{\text{eq}} \langle P_z^I \xrightarrow{\text{M2S}} P_S^I \rangle \langle P_S^I \xrightarrow{\text{S2M}} P_z^I \rangle \langle P_z^I \xrightarrow{\text{INEPT}} P_z^S \rangle \quad (\text{A.5})$$

There is a unitary bound on the conversion from thermal Zeeman polarization between two spins to singlet order between the same spins. At the low polarization level of a thermally polarized system, this transformation has a maximum amplitude of 2/3, and this factor is included in Eq. (5).

We approximate the oscillation between Zeeman polarization and singlet order on the I-spins as having an efficiency symmetric with respect to time reversal, and can therefore say:

$$\langle P_z^I \xrightarrow{\text{M2S}} P_S^I \rangle \simeq \sqrt{\frac{3}{2}} \frac{a_D}{a_C} \quad (\text{A.6})$$

The experimental value of the quantity in Eq. (A.6) is 0.31 for the 2,5-thiophenedicarboxylic acid sample used in the main paper. The efficiency of the ^{13}C S2hM conversion is then given by

$$\langle P_S^I \xrightarrow{\text{S2hM}} P_z^S \rangle \simeq \sqrt{\frac{3}{2}} \frac{\gamma_S}{\gamma_I} \frac{a_A}{a_B} \sqrt{\frac{a_C}{a_D}} \quad (\text{A.7})$$

where a factor of $\sqrt{\frac{3}{2}}$ is reintroduced to account for the maximum possible efficiency of the I-spin M2S. The experimental value of the quantity in Eq. (A.7) is 0.50 for the 2,5-thiophenedicarboxylic acid sample used in the main paper.

References

- [1] Albert W. Overhauser, Paramagnetic relaxation in metals, *Phys. Rev.* 89 (4) (1953) 689–700.
- [2] C. Russell Bowers, Daniel P. Weitekamp, Transformation of symmetrization order to nuclear-spin magnetization by chemical reaction and nuclear magnetic resonance, *Phys. Rev. Lett.* 57 (21) (1986) 2645–2648.

- [3] Thad G. Walker, William Happer, Spin-Exchange Optical Pumping of Noble-Gas Nuclei, 1997.
- [4] Joachim Bargon, The discovery of chemically induced dynamic polarization (CIDNP), *Helvet. Chim. Acta* 89 (10) (2006) 2082–2102.
- [5] Simon B. Duckett, Ryan E. Mewis, Application of parahydrogen induced polarization techniques in NMR spectroscopy and imaging, *Acc. Chem. Res.* 45 (8) (2012) 1247–1257.
- [6] Aaron J. Rossini, Alexandre Zagdoun, Moreno Lelli, Anne Lesage, Christophe Copéret, Lyndon Emsley, Dynamic nuclear polarization surface enhanced NMR spectroscopy, *Acc. Chem. Res.* 46 (9) (2013) 1942–1951.
- [7] Benno Meier, Jean-Nicolas Dumez, Gabriele Stevanato, Joseph T. Hill-Cousins, Soumya Singha Roy, Pär Håkansson, Salvatore Mamone, Richard C.D. Brown, Giuseppe Pileio, Malcolm H. Levitt, Long-lived nuclear spin states in methyl groups and quantum-rotor-induced polarization, *J. Am. Chem. Soc.* 135 (50) (2013) 18746–18749.
- [8] Soumya Singha Roy, Jean-Nicolas Dumez, Gabriele Stevanato, Benno Meier, Joseph T. Hill-Cousins, Richard C.D. Brown, Giuseppe Pileio, Malcolm H. Levitt, Enhancement of quantum rotor NMR signals by frequency-selective pulses, *J. Magn. Reson. (San Diego, Calif.: 1997)* 250C (2014) 25–28.
- [9] Jung Ho Lee, Yusuke Okuno, Silvia Cavagnero, Sensitivity enhancement in solution NMR: emerging ideas and new frontiers, *J. Magn. Reson. (San Diego, Calif.: 1997)* 241 (2014) 18–31.
- [10] Marina Carravetta, Ole Johannessen, Malcolm Levitt, Beyond the T1 limit: singlet nuclear spin states in low magnetic fields, *Phys. Rev. Lett.* 92 (15) (2004) 153003.
- [11] Giuseppe Pileio, Marina Carravetta, Malcolm H. Levitt, Storage of nuclear magnetization as long-lived singlet order in low magnetic field, *Proc. Natl. Acad. Sci. USA* 107 (40) (2010) 17135–17139.
- [12] Michael C.D. Tayler, Malcolm H. Levitt, Singlet nuclear magnetic resonance of nearly-equivalent spins, *Phys. Chem. Chem. Phys.: PCCP* 13 (13) (2011) 5556–5560.
- [13] Yesu Feng, Ryan M. Davis, Warren S. Warren, Accessing long-lived nuclear singlet states between chemically equivalent spins without breaking symmetry, *Nat. Phys.* 8 (11) (2012) 831–837.
- [14] T. Joseph Hill-Cousins, Ionut-Alexandru Pop, Giuseppe Pileio, Gabriele Stevanato, Pär Håkansson, Soumya S. Roy, Malcolm H. Levitt, Lynda J. Brown, Richard C.D. Brown, Synthesis of an isotopically labeled naphthalene derivative that supports a long-lived nuclear singlet state, *Org. Lett.* 9 (17) (2007) 2150–2153.
- [15] Irene Marco-Rius, Michael C.D. Tayler, Mikko I. Kettunen, Timothy J. Larkin, Kerstin N. Timm, Eva M. Serrao, Tiago B. Rodrigues, Giuseppe Pileio, Jan Henrik Ardenkjaer-Larsen, Malcolm H. Levitt, Kevin M. Brindle, Hyperpolarized singlet lifetimes of pyruvate in human blood and in the mouse, *NMR Biomed.* 26 (12) (2013) 1696–1704.
- [16] Roberto Buratto, Aurélien Bornet, Jonas Milani, Daniele Mammoli, Basile Vuichoud, Nicola Salvi, Maninder Singh, Aurélien Laguerre, Solène Passemard, Sandrine Gerber-Lemaire, Sami Jannin, Geoffrey Bodenhausen, Drug screening boosted by hyperpolarized long-lived states in NMR, *ChemMedChem* 9 (11) (2014) 2509–2515.
- [17] Alexey S. Kiryutin, Herbert Zimmermann, Alexandra V. Yurkovskaya, Hans-Martin Vieth, Konstantin I. Ivanov, Long-lived spin states as a source of contrast in magnetic resonance spectroscopy and imaging, *J. Magn. Reson.* 261 (2015) 64–72.
- [18] Jean-Nicolas Dumez, Pär Håkansson, Salvatore Mamone, Benno Meier, Gabriele Stevanato, Joseph T. Hill-Cousins, Soumya Singha Roy, Richard C.D. Brown, Giuseppe Pileio, Malcolm H. Levitt, Theory of long-lived nuclear spin states in methyl groups and quantum-rotor induced polarisation, *J. Chem. Phys.* 142 (4) (2015) 044506.
- [19] Gabriele Stevanato, Joseph T. Hill-Cousins, Pär Håkansson, Soumya Singha Roy, Lynda J. Brown, Richard C.D. Brown, Giuseppe Pileio, Malcolm H. Levitt, A nuclear singlet lifetime of more than one hour in room-temperature solution, *Angew. Chem. Int. Ed.* 54 (12) (2015) 3740–3743.
- [20] Gabriele Stevanato, Soumya Singha Roy, Joe Hill-Cousins, Ilya Kuprov, Lynda J. Brown, Richard C.D. Brown, Giuseppe Pileio, Malcolm H. Levitt, Long-lived nuclear spin states far from magnetic equivalence, *Phys. Chem. Chem. Phys.* 17 (8) (2015) 5913–5922.
- [21] Gabriele Stevanato, Long-Lived States in Multi-Spin Systems, PhD Thesis, Southampton (UK), 2015.
- [22] Soumya S. Roy, Philip Norcott, Peter J. Rayner, Gary G.R. Green, Simon B. Duckett, A hyperpolarizable ¹H magnetic resonance probe for signal detection 15 min after spin polarization storage, *Angew. Chem. Int. Ed.* 55 (50) (2016) 15642–15645.
- [23] Stuart J. Elliott, Lynda J. Brown, Jean-Nicolas Dumez, Malcolm H. Levitt, Long-lived nuclear spin states in monodeuterated methyl groups, *Phys. Chem. Chem. Phys.* 18 (27) (2016) 17965–17972.
- [24] Giuseppe Pileio, Singlet NMR methodology in two-spin-1/2 systems, *Prog. Nucl. Magn. Reson. Spectrosc.* 98–99 (2017) 1–19.
- [25] Mathias Haake, Johannes Natterer, Joachim Bargon, Efficient NMR pulse sequences to transfer the parahydrogen-induced polarization to hetero nuclei, *J. Am. Chem. Soc.* 118 (36) (1996) 8688–8691.
- [26] Sébastien Bär, Thomas Lange, Dieter Leibfritz, Jürgen Hennig, Dominik von Elverfeldt, Jan-Bernd Hövener, On the spin order transfer from parahydrogen to another nucleus, *J. Magn. Reson.* 225 (2012) 25–35.
- [27] Chong Cai, Aaron M. Coffey, Roman V. Shchepin, Eduard Y. Chekmenev, Kevin W. Waddell, Efficient transformation of parahydrogen spin order into heteronuclear magnetization, *J. Phys. Chem. B* 117 (5) (2013) 1219–1224.
- [28] Francesca Reineri, Tommaso Boi, Silvio Aime, Parahydrogen induced polarization of ¹³C carboxylate resonance in acetate and pyruvate, *Nat. Commun.*, 2015.
- [29] M. Goldman, H. Johannesson, Conversion of a proton pair para order into C-13 polarization by rf irradiation, for use in MRI, *Comp. Rend. Phys.* 6 (4–5) (2005) 575–581.
- [30] Stephen Kadlecsek, Kiarash Emami, Masaru Ishii, Rahim Rizi, Optimal transfer of spin-order between a singlet nuclear pair and a heteronucleus, *J. Magn. Reson.* 205 (1) (2010) 9–13.
- [31] Maurice Goldman, Haukur Jóhannesson, Oskar Axelsson, Magnus Karlsson, Design and implementation of ¹³C hyper polarization from para-hydrogen, for new MRI contrast agents, *Comp. Rend. Chim.* 9 (3–4) (2006) 357–363.
- [32] Stephen J. DeVience, Ronald L. Walsworth, Matthew S. Rosen, Preparation of nuclear spin singlet states using spin-lock induced crossing, *Phys. Rev. Lett.* 111 (17) (2013) 173002.
- [33] James Eills, Gabriele Stevanato, Christian Bengs, Stefan Glöggler, Stuart J. Elliott, Javier Alonso-Valdesueiro, Giuseppe Pileio, Malcolm H. Levitt, Singlet order conversion and parahydrogen-induced hyperpolarization of ¹³C nuclei in near-equivalent spin systems, *J. Magn. Reson.* 274 (2017) 163–172.
- [34] Gabriele Stevanato, Alternating delays achieve polarization transfer (ADAPT) to heteronuclei in PHIP experiments, *J. Magn. Reson.* 274 (2017) 148–162.
- [35] Malcolm H. Levitt, Singlet nuclear magnetic resonance, *Annu. Rev. Phys. Chem.* 63 (2012) 89–105.
- [36] R.R. Ernst, G. Bodenhausen, A. Wokaun, Principles of Nuclear Magnetic Resonance in One and Two Dimensions, Oxford University Press, Oxford, 1987.
- [37] S. Vega, Fictitious spin-1/2 operator formalism for multiple quantum nmr, *J. Chem. Phys.* 68 (1978) 5518–5527.